Journal of Engineering Science and Technology
7th EURECA 2016 Special Issue July (2018) 13 - 26

EFFECT OF SIZE AND SHAPE OF SIDE MIRRORS ON THE DRAG OF A PERSONAL VEHICLE

ABDULKAREEM SH. MAHDI AL-OBAIDI*, STEPHANIE LAI SHEN AI, LIM CHIN HONG

School of Engineering, Taylor's University, Taylor's Lakeside Campus,
No. 1 Jalan Taylor's, 47500, Subang Jaya, Selangor DE, Malaysia
*Corresponding Author: Abdulkareem.mahdi@taylors.edu.my

Abstract

This study aims to evaluate the effect of the size and shape of side mirrors on the drag of a personal vehicle. In running conditions of vehicles, the side mirror contributes to the increase of drag, hence increasing the fuel consumption. However, the side mirror only contributes to the drag when velocity is greater than 60 km/h. This study was carried out on a locally manufactured vehicle, the Perodua Myvi and its side mirrors. The average drag coefficients of a Perodua Myvi and its standard mirror were calculated as 0.354 and 0.175, respectively. The side mirror comprises of 3% of the total frontal area of the Perodua Myvi. The removal of standard side mirrors reduces the total drag coefficient of the vehicle by 4.9%. To analyse the effect of the size and shape, three parameters of side mirrors; height of foot, scale factor, and radius of housing curvature, were investigated using Computational Fluid Dynamic simulation. The meshing and solution methods were verified with published papers. The study was conducted at subsonic speeds with Mach number less than 0.1. The simulation was performed at a range of velocities between 80 km/h (22.22 m/s) to 120 km/h (33.33 m/s). The results obtained from the simulation were validated with published results and showed that at low subsonic speeds, the drag coefficient of the car is almost constant. A shorter side mirror mount would decrease the drag coefficient of the side mirror by 1%-5%. In addition, a smaller side mirror produces a lower drag coefficient of the side mirror by 14-43%. Finally, increasing the radius of housing curvature would decrease the drag coefficient of the side mirror.

Keywords: Computational Fluid Dynamics, Drag coefficient, Perodua Myvi, Side mirror, Subsonic.

1. Introduction

Side mirrors can be commonly found mounted onto the exterior of vehicles. The side mirror functions as a visual aid to view the parameters of the car. Otten [1] conducted a survey and found the average frontal area of a pair of side mirrors consists of 2-3% of the overall frontal area. In running conditions of the vehicle, the side mirror contributes to the drag of the vehicle. The side mirror only contributes to the drag when the velocity is greater than 60 km/h [2].

Aerodynamic drag is the force opposing the forward motion of a moving vehicle. Viscous force is the main contributor to drag at lower velocities. Therefore, skin friction drag is the main source of aerodynamic drag in a vehicle at low velocities [3]. However, pressure drag is a main source of drag at cruising speeds. Pressure drag is present when a shape changes abruptly. Pressure drag at the front of a vehicle is found to be higher than the rear [4]. Aerodynamic drag can be reduced by streamlining the body, as it is highly dependent on an object's shape. Magazoni et al. [5] found that the upper body of a vehicle experiences 45% of aerodynamic drag force. One of the components found in the upper body that contributes to drag is the side mirror. Turbulent wake is formed at the rear of the side mirror due to its shape. The total drag produced by side mirrors is 2-7% of the total drag of a vehicle [6]. Complex aerodynamic characteristics such as drag coefficient can be calculated using Eq. (1) in which F_D can be obtained through experiments.

$$F_D = C_D \frac{1}{2} \rho V^2 A \tag{1}$$

where, F_D is the drag force, C_D is the drag coefficient, ρ is the density of air, A is the frontal area, and V is the velocity of the object.

Olsson [6] numerically studied the drag coefficient of a simplified Mercedes-Benz A-class with no interior components or engine compartments. The author analyses the optimisation of the side mirrors that adheres to the law and regulations of European Union Law. Vibration noise factors were excluded from this study. Olsson studied ten different cases, which such as including the car with mirror, without mirror, using a reference mirror, different housing curvatures and varying gaps. The CFD simulation was conducted using PowerCASE software. The simulation results were validated with wind tunnel experiment. The CFD simulation shows a 13% percentage error as compared to wind tunnel results. The study concluded that modified side mirror produces an up wash effect in the rear front, which results in a reduction of drag. Olsson also found that a combination of two different modifications that individually reduces the drag can together produce a worse drag.

Batchelder [7] conducted research with a Smart Fortwo on the different components, which enhances the aerodynamic shape of the vehicle. The author studied side mirrors, stock style wheels, door handle, antenna and wheel well covers. The car was meshed using TGrid and imported into FLUENT to conduct the simulation. The removal of the side mirror reduces the drag coefficient by 4.8%.

Buscariolo and Roshilho [8] considered the applications of side mirror removal and the implementation of outside rear-view cameras using CFD simulation. The research conducted focused on the drag coefficient in respect to the frontal areas of a car. Four cases were studied including car with mirror, without mirror, and two concepts of outside rear view camera housing. The turbulence model used was k-ε

to establish pressure, wake profile and drag coefficient. The removal of side mirror and two implementation of camera installation reduces the drag coefficient by 1% and 0.4% respectively.

Ramdan and Lim [9] conducted a research to determine the fuel economy of a Perodua Myvi within the city and on highways. MATLAB backward-facing discretized simulation was used to solve the fuel consumption of the vehicle. Experiments were physically conducted to compare with the results obtained numerically. The simulation shows an average error percentage of 13% as compared to the experiments conducted. The results obviously showed that the highway routes produce a better fuel economy as it travels constantly at a cruising speed. Similarly, Shah and Mahmood [10] analysed the effect of side view mirror on fuel efficiency. Two types of mirror geometry were considered, a 13-cm diameter flat back and hemispherical back mirror. The drag coefficient was solved analytically travelling at an average speed of 60 km/h and 120 km/h. The hemispherical back mirror produces a lower fuel consumption, which saves 7.33 and 29.3 liters of petrol a year respectively.

The present paper aims to determine the effect of size and shape of side mirrors on the drag of a personal vehicle. First, the study will consider how the size and shape of side mirrors affect the drag by comprehending the fundamental background of fluid mechanics and aerodynamics using numerical analysis. Mirror optimisation is carried out to determine the best shape and size of a side mirror that produces a minimum drag. The design process of the side mirror should adhere to the legal demands of Malaysia. The research parameters are governed by the scope of study. A clean simplified side mirror, without interior or exterior components, was studied. Only personal vehicles such as sedans and hatchback are considered. The drag coefficient is determined numerically using CFD application. Lastly, the design of a side mirror must abide with the legal demands and regulations of Malaysia, taken from section 11(2) of 11. Economic Commission for Europe of the United Nations [11], which states that the dimensions of the main exterior rear-view mirrors for Classes II and III. A personal vehicle falls under the category M1 (carriage of passengers no more than eight seats) of Class III (small main side mirror).

2. Research Methodology

This section discusses the method in conducting this research. The discussion contains justification of each task and the configurations used for this study.

2.1. 3-D Geometry modelling

Based on the scope derived for this study, a personal vehicle was chosen from a locally manufactured car, the Perodua Myvi. The second generation of Perodua Myvi 1.3 EZi was released in 2012. This model was chosen as the test model for this research due to its relevance in studying a localized vehicle. The car was constructed by surface modelling using SolidWorks as shown in Fig. 1(a). The vehicle and side mirror were separately modelled. The vehicle without side mirror was modelled with ground clearance, length, width and height of 0.218 m, 3.576 m, 1.605 m and 1.31 m, respectively. However, due to the complexity of shape and limitation of time, a simplified model was produced by outlining the general shape of the existing test model as shown in Fig. 1(b). The simplified model was modelled

with ground clearance, length, width, height of 0.207 m, 3.558 m, 1.507 m and 1.487 m, respectively.

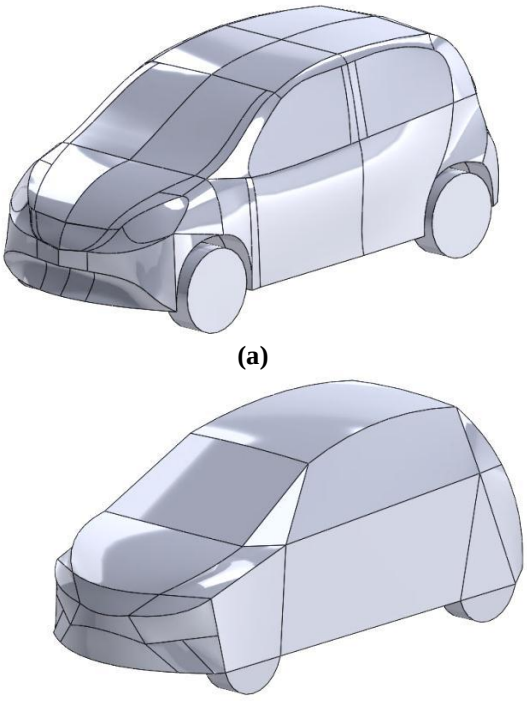

(a)

(b)

Fig. 1. Myvi Configuration (a) Modelled (b) Simplified.

The frontal area for the original and simplified model measures to be 2.06 m^2 and 1.97 m^2 respectively. The frontal area of the simplified model has an average percentage error of 4.4% compared to the first model.

The dimensions of the side mirror were measured with a physical model. The side mirror was modelled with SolidWorks as shown in Fig. 2. The frontal area of two modelled side mirrors is measured to be 3% of the total frontal area of the simplified car. This value is verified with the survey conducted by Otten [2]. As this research studies the effect of size and shape of side mirror to drag, three different designs were modified from the standard side mirror. The designs will be further discussed under results and calculations.

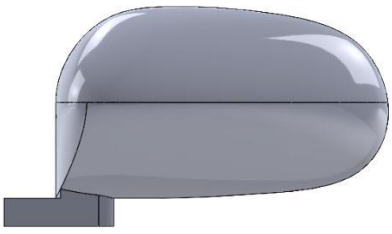

Fig. 2. Standard side mirror.

2.2. Numerical method

2.2.1. Geometry modelling

To simulate wind tunnel conditions of a stationary car with fluid flow, an enclosed domain was created. The enclosed domain is defined by a half-body model. The model is assumed symmetric with a steady flow. Therefore, a large enclosed domain is produced to create an undisturbed inlet and outlet flow. To obtain accurate results, the recommended dimensions of an enclosed domain should be 30 times of the car's length, *L*. However, with the limitation of time, the dimension units of the enclosed domain were taken from the studies of [4, 12]. The dimensions were standardised with *L*. The inlet and outlet distance are at a distance of 2*L* and 4*L* as shown in Fig. 3. A body of influence was created to direct the focus to the vehicle. The body of influence was placed at a distance of 0.5 m, 2 m and 1.25 m from the front, rear and side of the car respectively. The enclosed domain and body of influenced was placed slightly above the *x*-axis, intersecting the tires of the model. This is to ensure there is no fluid passing the tires to simulate real running conditions. In addition, an enclosed domain was done similarly for the side mirror with specific dimensions as in Fig. 4. The side mirror is suspended 2 m from the ground.

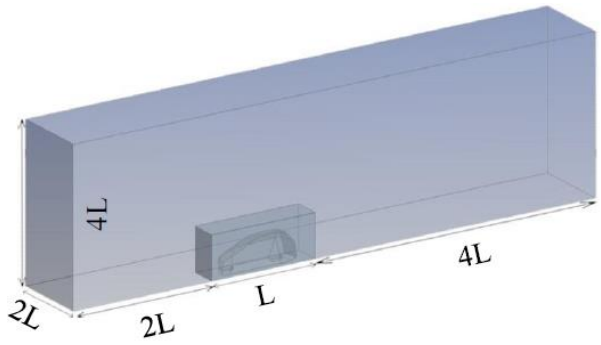

Fig. 3. 3-D enclosed domain.

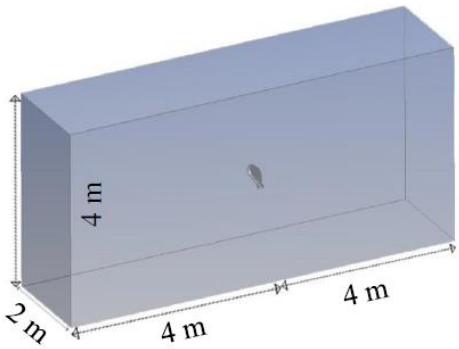

Fig. 4. 3-D enclosed domain.

2.2.2. Meshing method

Meshing is an important factor in producing accurate results. An exercise was conducted prior to this study with NACA 4415 at Reynolds number 3×10^6 for 0°

angle of attack. This exercise was done to validate the meshing method used in studying the drag coefficient. The results were verified with a NACA report [13] and obtained an error percentage of 19%.

Tetrahedral mesh was used due to its proximity and curvature of the vehicle. The global mesh size settings had a coarse relevance center, which produces an appropriate mesh that creates finer mesh around the curvatures of vehicle's body and produces large mesh sizes further away from the body. The default mesh was improved to capture the flow around the vehicle. This study uses a combination of meshing method from [4, 12, 14]. Firstly, face sizing was applied to the faces of the vehicle to refine the mesh of the faces of the vehicle. The number of elements in the vehicle increases as the size of each element decreases as compare to the default mesh. Secondly, two inflation layers were added. The first inflation layer was around the vehicle to capture the boundary effects of flow around the vehicle. The second inflation layer on the wind tunnel floor. This would reduce numerical diffusion and provide good analysis of flows near the floor and the vehicle [15]. Both inflation have a first layer thickness of 0.005 m with a seven layers at a growth rate of 1.3. Lastly, body sizing was applied on the body of influence as a local refinement. The majority of elements are found around the vehicle and wake region as shown in Fig. 5.

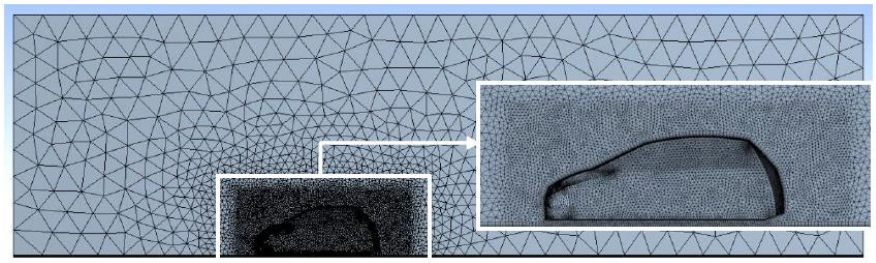

Fig. 5. Final mesh generation.

Similarly, the standard side mirror uses the same global mesh size setting as the vehicle. The inflation was generated on the mirror with a growth rate of 1.2. The edge sizing was applied to the edges of the mount. Figure 6 shows the details of mesh on the side mirror.

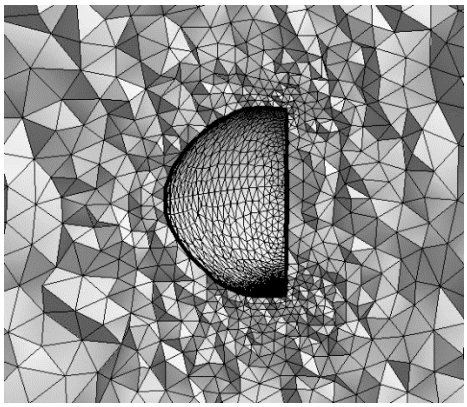

Fig. 6. Mirror name selections.

2.2.3. Numerical setup

Navier-Stokes equations are used together with k-ε turbulence model to solve the airflow. Navier-Strokes equations consist of governing equations such as continuity equation, Eq. (2), and momentum equations, Eqs. (3)-(5).

$$\frac{\partial \rho}{\partial t} + \nabla \cdot (\rho V) = 0 \tag{2}$$

$$\frac{\partial \rho u}{\partial t} + \nabla \cdot \rho u V = -\frac{\partial P}{\partial x} + \nabla \cdot (\mu \nabla u) + S_{m,x} \tag{3}$$

$$\frac{\partial \rho v}{\partial t} + \nabla \cdot \rho v V = -\frac{\partial P}{\partial y} + \nabla \cdot (\mu \nabla v) + S_{m,y} \tag{4}$$

$$\frac{\partial \rho w}{\partial t} + \nabla \cdot \rho w V = -\frac{\partial P}{\partial z} + \nabla \cdot (\mu \nabla w) + S_{m,z} \tag{5}$$

where u, v and z are the components of velocity vector in x, y and z axes, ρ is the air density, P is static pressure and $S_{m,x}$, $S_{m,y}$,and $S_{m,z}$ are source terms for x, y and z-components.

The flow is considered incompressible as the Mach number is less than 0.3. The fluid is set to air with its default values of density and viscosity. The k-ε turbulence model was selected with standard wall treatment to follow the conditions of a wind tunnel. The turbulence model was selected based on the setup by Magazoni et al. [5] and Buscariolo and Rosilho [8]. Besides, k-ε turbulence model is a suitable model due to the ground clearance which emulates an internal flow, whereas, the Spalart Allmaras turbulence model was selected for the side mirror as it is suspended on air and attached to the walls. The body of the vehicle, side mirror and floor of wind tunnel were set to no slip wall condition. The symmetry was set as a symmetry plane. The inlet specified the velocities ranging from 80 km/h to 120 km/h, with intervals of 10 km/h. However, the velocity input in FLUENT is in m/s. The output boundary condition uses an outlet pressure of 0 Pa. Pressure far field was not selected due to the intersection between the wheels and wind tunnel floor, which prevents the selection of pressure far field.

The simulations were conducted at varying speeds for the following cases.

Case 1: Vehicle without mirror.
Case 2: Isolated standard side mirror.
Case 3: Three different designs of an isolated side mirror.

2.2.4. Study cases

Table 1 represents the different designs of side mirror studied in this research. A range was given to each parameter to determine an optimum design that produces minimum drag coefficient. The parameters were set by non-dimensional ranges starting from 70% up to 130%, with 10% increment. Abbreviations are used to identify the design as Height of Foot (HF), Scale Factor (SF) and Radius of Housing Curvature (RC) is equivalent to the standard mirror.

Table 1. Parameters of case study.

Parameters	Range of Application
Height of Foot (HF)	0.7 HF ≤ HF ≤ 1.3 HF
Scale Factor (SF)	0.7 SF ≤ SF ≤ 1.3 SF
Radius of Housing Curvature (RC)	0.7 RC ≤ RC ≤ 1.3 RC

Height of foot (HF)

The first parameter, height of foot, represents the height and thickness of the side mirror's mount. Six different heights were simulated at various speeds. Other components of the side mirror were kept constant. Figure 7 represents three ranges of different heights of foot. The range $0.7HF \leq HF \leq 1.3HF$ ranges from 140 mm to 260 mm respectively.

0.9 HF **0.8 HF** **0.7 HF**

Fig. 7. Height of foot.

Scale factor (SF)

The second parameter changes the scale of the side mirror only, as the dimensions of the mount remains constant. This is to study the effect of size on the drag of a side mirror. Figure 8 shows three ranges of different scale factors. The range $0.7SF \leq SF \leq 1.3SF$ ranges from 164.50 mm to 305.50 mm respectively.

.

0.9 SF **0.8 SF** **0.7 SF**

Fig. 8. Scale factor.

Radius of housing curvature (RC)

The last parameter considered is the curvature of the housing. The radius of housing curvature was adjusted as shown in Fig. 9. Six different housing curvatures were simulated. The frontal area of the mirror housing was kept constant. The cases are $0.7RC \leq RC \leq 1.3RC$ ranges from 69.35 mm to 107.68 respectively.

0.9 RC **0.8 RC** **0.7 RC**

Fig. 9. Radius of housing curvature.

2.2.5. Assumptions

Few assumptions were established at the beginning of this research are stated as below.

- The effect of the ground is not considered.
- The computational domain is to replicate the setup of a wind tunnel.
- The car configuration is approximately due to the complexity of the shape, which requires more time.
- The side mirror is perpendicular to the airflow. Inclination angle is not considered.

2.2.6. Drag coefficient calculation of side mirror

The subtraction of drag coefficient of a vehicle with mirror and without mirror equals to the drag coefficient of an isolated side mirror. However, this study simulates an isolated mirror separated from the vehicle. Therefore, a ratio must be used to calculate the drag coefficient of a side mirror in respect to the whole vehicle in Eq. (6).

$$C_{D(mirror)} = C_{D(value\ obtained\ from\ CFD)} \frac{A_{Two\ mirrors}}{S_{ref}} \quad (6)$$

where $C_{D(mirror)}$ is the drag coefficient of mirror, $C_{D(\text{value } obtained\ from\ CFD)}$ is the drag coefficient solved by ANSYS FLUENT, $A_{two\ mirrors}$ is the frontal area of each side mirror, and S_{ref} is the frontal area of the vehicle without mirrors. The frontal areas for both mirrors and vehicle are measured using SolidWorks.

3. Results and Discussion

3.1. The car

The relation between drag coefficient and velocity of the car is shown in Fig. 10. It can be observed that the highest contributor to drag coefficient is from pressure drag. Figure 10 shows a constant drag coefficient through different velocities. This was validated, as the drag coefficient is constant at low Reynolds number [3]. The drag coefficient of a Perodua Myvi is said to be between 0.32-0.35 [9, 16, 17]. However, these values are not verified as the official provider does not state the drag coefficient of this model.

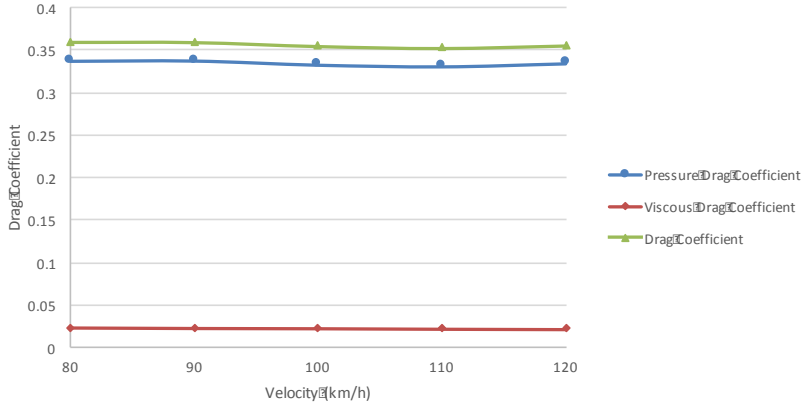

Fig. 10. Drag coefficient vs. velocity.

Figure 11 exhibits the pressure distribution of a car running at 100 km/h. The pressure is highest at the front of the vehicle. The pressure behind the vehicle is lower

than the front. Simultaneously, velocity is lowest at the front of the vehicle due to stagnation point as shown in Fig. 12. The boundary layer was created over the vehicle with an inflation mesh. The wake can be found when air exits the rear of the vehicle.

Figure 13 displays the pressure distribution of the vehicle. The fluid compresses at the front of the vehicle, resulting in high pressure and a downward force. Simultaneously, air is travelling along the side of the vehicle at atmospheric pressure, forming a lower pressure than the front.

Fig. 11. Pressure distribution over symmetric plane

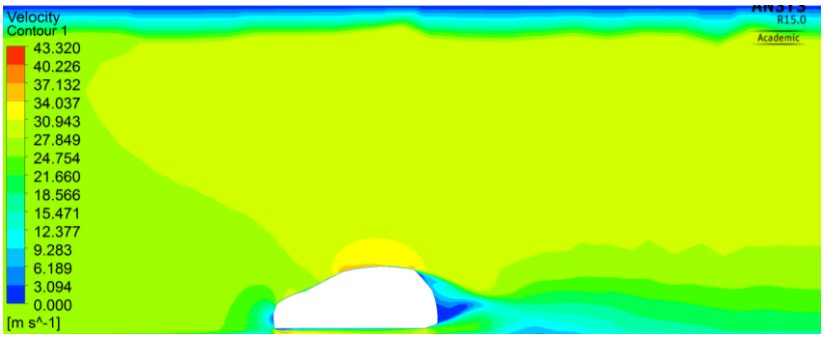

Fig. 12. Velocity distribution over symmetric plane

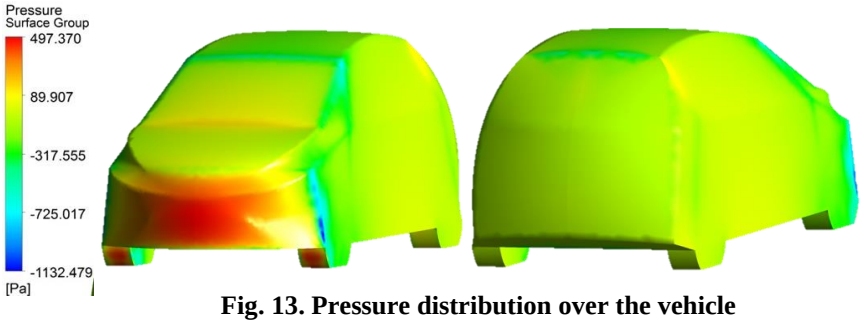

Fig. 13. Pressure distribution over the vehicle

3.2. Side mirror

3.2.1. Standard mirror

Figures 14 and 15 represent the pressure contour and velocity vector profile of a standard side mirror at 100 km/h. The standard mirror shows high pressure when the flow reaches the front surface of the side mirror, this reduces the airflow speed

and reducing the boundary flow separation. The standard mirror contributes to approximately 4.9% of drag reduction to the whole vehicle.

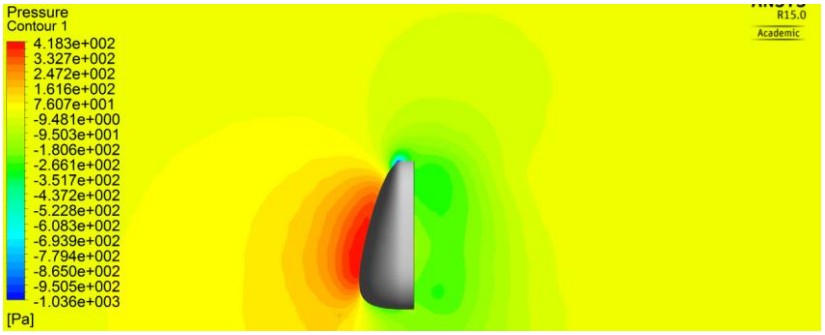

Fig. 14. Pressure contours over the side mirror from top view.

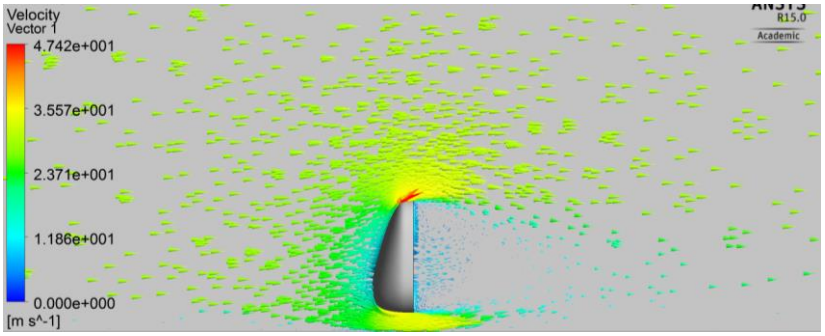

Fig. 15. Velocity vector over the side mirror from top view.

3.2.2. Height of foot

Figure 16 shows the results obtained for the parameter height of foot at different velocities. Based on Fig. 16, a similar trend is observed for all ranges. The drag coefficient increase when height of the mount increases. The flow separation between the wall of a wind tunnel and the side mirror slightly affects the total drag coefficient of a side mirror. However, the reduction of thickness has no significant in the reduction of drag coefficient. Reducing the thickness might affect the stability of the side mirror and may produce vibration.

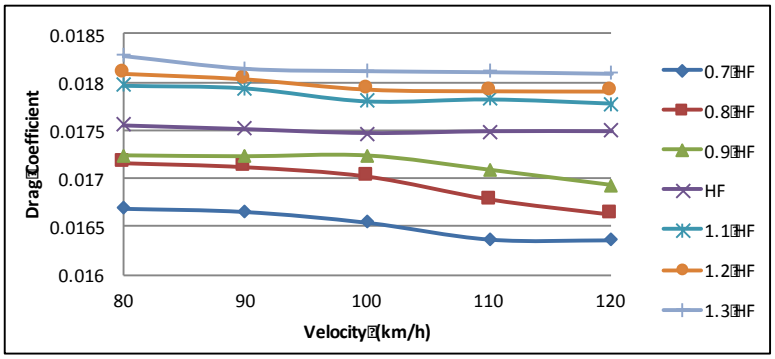

Fig. 16. Drag comparison between different height of foot and velocity.

3.2.3. Scale factor

Figure 17 illustrates the results from varying the scale factor of the side mirror at different velocities. Figure 17 clearly shows a consistent trend through all the ranges. Drag coefficient decreases with a smaller scaled side mirror. Therefore, a smaller area would result in a lower drag. This parameter shows a larger contribution to the reduction of drag coefficient than the height of foot parameter.

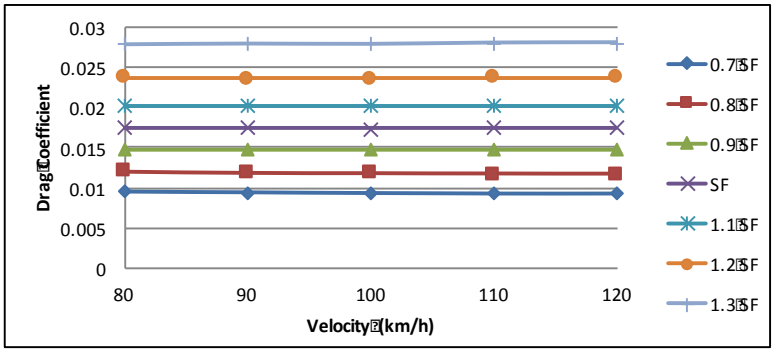

Fig. 17. Drag comparison between different scale factors and velocity.

3.2.4. Radius of housing curvature

Figure 18 exhibits the results from different housing curvatures based on the standard mirror. A similar trend is observed, however the effect of drag to this parameter is the reverse of Figs. 16 and 17. A flatter housing is produced when the radius of housing curvature decreases, thus the drag coefficient increases. There is no major significance in the reduction of drag coefficient. However, the ranges in Fig. 18 have exceeded the results for standard side mirror. This result occurred as all these parameters shares the same frontal area as the standard side mirror.

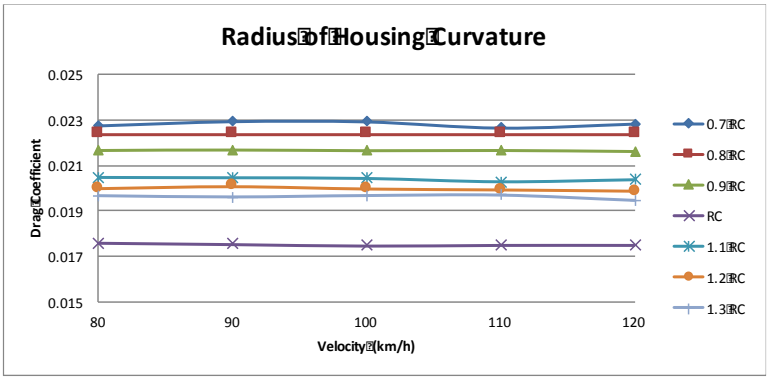

Fig. 18. Drag comparison between different radius of housing curvature and velocity.

4. Conclusions

The effect of the size and the shape of the side mirror in the drag of a personal vehicle was studied numerically. The frontal area of both side mirrors consists of

3% of the total frontal area of the vehicle. The standard mirror reduces 4.9% the drag coefficient of a Perodua Myvi. Three different parameters were considered to study the drag effect. The effect of these parameters is summarized as follows:

- The decrease of height and thickness of the mount reduces the drag coefficient of the side mirror.
- The decrease of volume of the side mirror reduces the drag coefficient of the side mirror.
- The increase of radius of housing curvature reduces the drag coefficient of the side mirror.
- The drag coefficient is approximately constant at low subsonic speeds.

Acknowledgement

Throughout this whole research process, various guidance, supervision and assistance was offered. Much gratitude and appreciation to Shahrooz Eftekhari, Wesley Otten and Abdul Sattar Khathman as research partners.

Nomenclatures

A	Frontal area, m^2
$A_{two\ mirrors}$	Ratio of diameter of nose blunting to cylinder diameter ($2r_o/d$)
C_D	Drag coefficient of the car
$C_{D(mirror)}$	Drag coefficient of side mirror
F_D	Drag force, N
L	Length of car, m
V	Velocity of fluid flow, m/s
S_{ref}	Reference area of car (maximum frontal cross-section), m^2

Greek Symbols

ρ	Density, kg/m^3

Abbreviations

CFD	Computational Fluid Dynamics
HF	Height of foot
NACA	National Advisory Committee for Aeronautics
RC	Radius of housing curvature, m
SF	Scale factor

References

1. Otten, W. (2016). *Aerodynamic analysis of a personal vehicle side mirror*. Final Year Project, Interim Report, Taylor's University, Malaysia. (Private Communication).
2. Barnard, R.H. (2009). *Road vehicle aerodynamic design*. St Albans, United Kingdom: Mechaero Publishing.
3. Anderson, J.D. (2010). *Fundamentals of aerodynamics.* Avenue of Americas, New York: McGraw-Hill.

4. Birwa, K.S.; Rathi, N.; and Gupta, R. (2013). Aerodynamic analysis of Audi A4 Sedan using CFD. *Journal of the Institution of Engineering* (*India*), 94(2), 105-111.
5. Magazoni, F.C.; Maruyama, F.K.; Buscariolo, F.F.; Alves, J.C.L.; and Volpe, L.J.D. (2015). Aerodynamic shape improvement for driver side view mirror of hatchback vehicle using adjoint optimization method. *SAE Technical Paper Series*, 36-0156.
6. Olsson, M. (2011). *Designing and optimizing side view mirrors.* Master's thesis, Chalmer University of Technology, Sweden.
7. Batchelder, J.H. (2009). *A CFD investigation of potential aerodynamic enhancements to a microcar class vehicle.* Master's thesis, Rensselaer Polytechnic Institute, USA.
8. Buscariolo, F.F.; and Rosilho, V. (2013). Comparative CFD study of outside rearview mirror removal and outside rearview cameras proposals on a current production car. *SAE Technical Paper Series*, 36-0298.
9. Ramdan, M.I.; and Lim, C.P. (2015). Fuel economy comparison of Perodua Myvi passenger vehicle on Malaysia city and highway drive cycles. *Journal of Scientific Research and Development*, 2(13), 76-82.
10. Shah, A.; and Mahmood, S.M. (2014). Study of side view mirrors design on the fuel consumption of a car. *Global Sci-Tech*, 6(4), 224-227.
11. Economic Commission for Europe of the United Nations (2013). *Uniform provisions concerning the approval of devices for indirect vision and of motor vehicles with regard to the installation of these devices.* Addendum 45: Regulation 46.
12. Damjanovic, D.; Kozak, D.; Zivic, M.; Ivandic, Z.; and Baskaric T. (2010). CFD analysis of concept car in order to improve aerodynamics. *Keynote Address at International Scientific and Expert Conference TEAM*, Kecskemet.
13. Abbott, I.H.; Doenhoff, A.E.V.; and Stivers, L.S.J. (1945). Summary of airfoil data. *Report No. 824*.
14. Cakir, M. (2012). *CFD study on aerodynamic effects of a rear wing/spoiler on a passenger vehicle.* Master's thesis, Santa Clara University, USA.
15. Lanfrit, M. (2005). *Best practice guidelines for handling automotive external aerodynamics with FLUENT.* Fluent Deutschland GmbH, Germany.
16. Zal, P. (2012). *2012 Perodua Myvi 1.3 EZi (model for Asia) specifications and performance data review*. Retrieved on 17 Oct 2016 from: http://www.automobile-catalog.com/car/2012/1224230/perodua_myvi_1_3_ezi.html
17. One Shift (2012). *Perodua Myvi EZI (A).* Retrieved on 17 Oct 2016 from: http://www.oneshift.com/new_cars/car-specs.php?pid=2090